Ex vivo Expanded Human Regulatory T Cells Modify Neuroinflammation in a Preclinical Model of Alzheimer's disease

Alireza Faridar
Houston Methodist Hospital
Matthew Vasquez
Houston Methodist Hospital
Aaron D. Thome
Houston Methodist Hospital
Zheng Yin
Houston Methodist Hospital
Hui Xuan
Houston Methodist Hospital
Jing Hong Wang
Houston Methodist Hospital
Shixiang Wen
Houston Methodist Hospital
Xuping Li
Houston Methodist Hospital
Jason R. Thonhoff
Houston Methodist Hospital
Weihau Zhao
Houston Methodist Hospital
Hong Zhao
Houston Methodist Hospital
David R. Beers
Houston Methodist Hospital
Stephen T.C. Wong
Houston Methodist Hospital
Joseph C. Masdeu
Houston Methodist Hospital
Stanley Appel (✉ sappel@houstonmethodist.org)
Houston Methodist Hospital https://orcid.org/0000-0003-2747-6298

Research Article

Keywords: Alzheimer's Disease, Regulatory T cells, Inflammation, Adaptive Immune System, Microglia, Amyloid Pathology

Posted Date: June 7th, 2022

DOI: https://doi.org/10.21203/rs.3.rs-1639205/v1

Abstract

Background:

Regulatory T cells (Tregs) play a neuroprotective role by suppressing microglia and macrophage-mediated inflammation and modulating adaptive immune reactions. We previously documented that Treg immunomodulatory mechanisms are compromised in Alzheimer's disease (AD). *Ex vivo* expansion of Tregs restores and amplifies their immunosuppressive functions *in vitro*. A key question is whether adoptive transfer of *ex vivo* expanded human Tregs can suppress neuroinflammation and amyloid pathology in a preclinical mouse model.

Methods:

An immunodeficient mouse model of AD was generated by backcrossing the 5xFAD onto Rag2 knockout mice (5xFAD-Rag2KO). Human Tregs were expanded *ex vivo* for 24 days and administered to 5xFAD-Rag2KO. Changes in amyloid burden, microglia characteristics and reactive astrocytes were evaluated using ELISA and confocal microscopy. NanoString Mouse AD multiplex gene expression analysis was applied to explore the impact of *ex vivo* expanded Tregs on the neuroinflammation transcriptome.

Results:

Elimination of mature B and T lymphocytes and natural killer cells in 5xFAD-Rag2KO mice was associated with upregulation of 95 inflammation genes and amplified number of reactive microglia within the dentate gyrus. Following peripheral administration, *ex vivo* expanded human Tregs were detectable in the frontal cortex and dentate gyrus of 5xFAD-Rag2KO and reduced amyloid burden and reactive glial cells. Interrogation of inflammation gene expression documented down-regulation of pro-inflammatory cytokines (*IL1A&B, IL6*), complement cascade (*C1qa, C1qb, C1qc, C4a/b*), toll-like receptors (*Tlr3, Tlr4 and Tlr7*) and microglial activations markers (*CD14, Tyrobp,Trem2*).

Conclusions:

Ex vivo expanded human Tregs, with amplified immunomodulatory function, suppressed neuroinflammation and alleviated AD pathology in vivo. Our results provide preclinical evidences for Treg cell therapy as a potential treatment strategy in AD.

Background:

The discovery of risk genes involved in inflammation signaling (1–3), indicates that inflammation is critical for the onset and progression of Alzheimer's disease (AD). In AD transgenic mouse models, microglia is one of the initial responders to amyloid-β plaque deposits (4–6). Activation of microglial

pattern recognition toll-like receptors (TLRs) and intracellular NLRP3 inflammasomes induces tau hyperphosphorylation and aggregation (7–11). Subsequent release of truncated phosphorylated tau also enhances immune cell activation, promoting the release of inflammatory mediators and a self-propagating cascade of synaptic dysfunction, neuronal injury, and cell death (11–14). The structural integrity of the blood-brain barrier is also impaired in the presence of AD pathology (15–17), thereby permitting substantial crosstalk between the central nervous system (CNS) and peripheral immune system. Thus, circulating immune cells might reflect and contribute to AD pathogenesis (18–20). Regulatory T cells (Tregs) are a subset of T cells that play a neuroprotective role by suppressing inflammation in the blood and brain (21). We have previously documented that Treg immunomodulatory mechanisms are compromised in AD patients (22). We propose that compromise of the peripheral adaptive immune system, particularly the Treg population would further enhance neuroinflammation and contribute to the pathogenesis of AD.

Accumulating preclinical and clinical evidences suggest Tregs as a modifiable therapeutic target. *Ex vivo* expansion of dysfunctional Tregs in AD individuals not only restored but enhanced their immunosuppressive function (22). Restoration of Tregs is currently being translated into cell therapy for neurodegenerative disorders. Recently, our group has conducted a first-in-human Phase I trial of expanded autologous Treg infusions in Amyotrophic Lateral Sclerosis (ALS) (23). The study demonstrated safety and potential benefit of this treatment strategy, and a Phase II double blind, placebo-controlled study is currently underway. The promising therapeutic potential of autologous infusions of expanded Tregs in ALS raised the question as to whether a similar strategy would be of value in AD. In the current study, we investigated the impact of *ex vivo* expanded human Tregs on neuroinflammation and Aβ pathogenesis in a preclinical AD system.

The widely used 5xFAD mice model recapitulates early and aggressive features of AD pathology with sustained microglial activation, increased inflammation markers and abundant deposition of plaques at early ages (24, 25). To evaluate the role of the adaptive immune system on AD pathology, a mouse model of AD was generated by backcrossing the 5xFAD mouse onto a Rag2 knockout mouse (5xFAD-Rag2KO). The resulting mice lack T cells, B cells and natural killer (NK) cells. Eliminating these adaptive immune cells amplified reactive microglia and aggravated plaque deposition within the hippocampus. In the next step, *ex vivo* expanded human Tregs with remarkably enhanced immunosuppressive function were adoptively transferred to the immunodeficient 5xFAD-Rag2KO mice. This Rag2 KO mouse model is an appropriate host for xenogeneic human cell engraftment with minimal host versus graft reaction (26–31). Following peripheral administration, human Tregs were detectable in the frontal cortex and dentate gyrus. They effectively reduced numbers of reactive microglia and astrocytes, suppressed neuroinflammation transcriptome and alleviated amyloid burden.

Methods:

Generation of a Rag2 Il2rγ$^{-/-}$ knock out immune-deficient AD mouse model

All animal protocols were approved by the Methodist Research Institute's Institutional Animal Care and Use Committee in compliance with National Institutes of Health guidelines. Rag2 Il2rγ$^{-/-}$ double knock out mice were initially bred with purebred 5xFAD and strain-matched wild-type C57BL/6 mice to generate immune-deficient 5xFAD-Rag2KO and strain-matched WT-Rag2KO mice. The presence or absence of the Rag2 gene was determined by PCR using 250 ng of tail DNA and Eppendorf TaqDNA polymerase according to the manufacturer's instructions. The following primers were used: Rag A) 5´-GGGAGGACACTCACTTGC-CAG-3´ and Rag B) 5´ AGTCAGGAGTCTCCATCTCAC-3´ and Neo C) 5´-CGGCGG-GAGAACCTGCGTGCAA-3´. Homozygotic mice will have one 350 bp band. Heterozygotic mice will have 350 and 263 bp bands. Wild-type mice will have one 263 bp band.

Ex vivo expansion of human Tregs and passive transfer to mice

Human CD4^{+}CD25^{high} T lymphocytes were isolated from peripheral blood of a healthy subject using the Regulatory T Cell Isolation Kit (Miltenyi Biotec) according to the manufacturer's instructions. Tregs were suspended at a concentration of 1x10^{6} cells/ml in media containing 100nM of rapamycin (Miltenyi Biotec), 500 IU/ml IL-2 (Miltenyi Biotec) and DynabeadsTM Human Treg Expander (GibcoTM) at a 4:1 bead-to-cell ratio for 8 days (First stimulation). At day 8, beads were removed, and cells were resuspended in a culture medium containing 100 U/mL IL-2 and 100nM of rapamycin for 8 days. On day 16, Tregs were restimulated by adding Dynabeads expansion beads at a 1:1 bead-to-cell ratio for further 8 days. After the second stimulation, Tregs were harvested and washed on day 24. The Treg immunophenotype and suppressive function were assayed prior to injection to mice, as described previously (22) to confirm enhanced immunomodulatory function. 1x10^{6} ex vivo expanded Treg cells were suspended in a 200 µl of phosphate-buffered saline (PBS) and were passively transferred into 5-month-old 5xFAD-Rag2 KO and WT-Rag2 KO mice via tail vein injections. This treatment was repeated every 28 days for a total of 5 months and the mice were sacrificed at age 10 month.

RNA sample preparation and transcriptome analysis

Using Trizol reagent, followed by Direct-zol RNA MiniPrep Kit (Zymo Research), messenger RNA was extracted from medial temporal cortex of mice. Quantitative PCR experiments were performed using a One-Step RT-PCR kit with SYBR Green and run on the Bio-Rad iQ5 Multicolor Real-Time PCR Detection Systems. For mouse neuroinflammation panel analysis, 770 transcripts were quantified with the NanoString nCounter multiplexed target platform (www.nanostring.com). nCounts of mRNA transcripts were normalized using the geometric means of 10 housekeeping genes (Csnk2a2, Ccdc127, Xpnpep1, Lars, Supt7l, Tada2b, Aars, Mto1, Tbp, and Fam104a).

Protein extraction and ELISA assay

The right hemisphere samples were homogenized in a 2% SDS lysis buffer (SDS, NaCl 150 mM and Triton™ 1%) containing phosphatase (Pierce) and protease (Roche) inhibitors. After centrifugation (60 min, 100,000 x g, 4°C), the supernatant was collected (SDS extract) and the protein concentration was quantified. 70% formic acid in water was added to the pellet and the supernatant was collected after

sonication and centrifugation (FA extract). Soluble (SDS extract) and insoluble (FA extract) Aβ40 and Aβ42 were measured using Amyloid beta Human ELISA Kit (Invitrogen).

Immunofluorescence staining

Splenocytes were isolated from spleens for flow cytometric analysis. Antibodies against the following surface markers were provided by: CD3 FITC (eBioscience™), CD4 PE (eBioscience™), CD8a Alexa Fluor 700 (eBioscience™), CD161 APC (eBioscience™) and CD19 PE-Cy5 (eBioscience™). Dead cells were stained by LIVE/DEAD® Fixable Blue Dead Cell Stain Kit (Life Technology). For immunohistochemical brain analyses, the left cerebral hemisphere was dissected and post-fixed in 4% paraformaldehyde in 0.1 M PBS for 2 days. Brains were cryoprotected by incubation in a 30% sucrose/0.1 M PBS solution. Sagittal brain sections were cut on a freezing microtome (Leica) and collected serially. Immunohistochemistry was performed on free-floating microtome-cut sections (10 µm in thickness). Sections were incubated with different antibodies: anti-mouse Iba1 (Polyclonal, 1:1000 Wako), anti-mouse CD68 (Clone FA-11, 1:200; BioRad), β-Amyloid (Clone 6E10, 1:1000; BioLegend), β-Amyloid 1-42 (polyclonal, 1:100; Millipore), anti-mouse GFAP (Clone GA-5, 1:100, Novus Biological) anti-human CD3 (Clone: CD3-12, 1:100, abcam) and anti-human Foxp3 (Clone 236A/E7, 1:100, Invitrogen). Appropriate secondary antibodies (Alexa Fluor 488, 594, or 647; Invitrogen) were used followed by incubation with DAPI.

Confocal image quantification

After immunofluorescence staining, images were captured using a Nikon A1 laser scanning confocal microscope. The system uses a galvanometer scanner with a 20x Plan Apo objective, and a pinhole set to 1.2 Airy Unit. Laser power, numeric gain and magnification were kept constant between animals to avoid potential technical artefacts. NIS Elements Version 5.11.01 was used to quantify mean intensity of fluorescence, number of immunoreactive cells, and size of plaques. The area we analyzed were defined as an actual single image field. Since each image was 1024x1024 pixels with a resolution at 0.63um/pixel, we measured the amount of immunoreactive cells in a 416,179.81 um2 area of frontal cortex or dentate gyrus. Intensity and size thresholds were applied for Aβ, Iba1, CD68 or GFAP positive cell quantification. All absolute quantifications were performed at ×20 magnification.

Statistical analysis

Mice were grouped based on genotype and treatment. The analyses, including immunohistochemistry staining, ELISA and transcriptome analysis were performed by other independent investigators. Statistical analysis was performed using Prism 7.0 (GraphPad Software). The significance of group comparisons was tested using paired or unpaired student's t-test (for two groups) or one-way ANOVA (for more than two groups). Data were expressed as Mean ± SEM and p values less than 0.05 were considered significant. For transcriptome analysis, nSolver software was used for background subtraction and normalization of data. Statistical analysis on the normalized expression profiles, including one-way ANOVA and multiple comparison using Tukey's range test, were carried out using the Statistics and Machine Learning Toolbox in MATLAB R2020a. Volcano plots of differential expressed genes data were

plotted using GraphPad Prism. Gene enrichment analysis was performed using Ingenuity pathway analysis (IPA).

Results:

Treg administration alleviates amyloid burden in immunodeficient AD mice

We generated 5xFAD-Rag2KO and WT-Rag2KO mice by backcrossing the 5xFAD and C57BL/6J mice onto a Rag2 Il2rγ$^{-/-}$ double knock out background. We have documented lack of adaptive immune system including CD4 and CD8 T cells, B cells and NK cells in transgenic Rag2 KO mice (Supplementary Fig. 1). These cells are the key immune components involved in xenogeneic cell rejection. Strain-matched immunocompetent AD and wild-type (WT) mice, termed 5xFAD-WT and WT-WT respectively, were also developed. Highly sensitive multiplex ELISA was performed to quantify the burden of SDS-soluble and formic acid (FA) treated insoluble Aβ within the brains of immunocompetent 5xFAD-WT and immunodeficient 5xFAD-Rag2KO mice (n = 10/group; sex-balanced). In the absence of the adaptive immune system, there was a trend toward increased levels of Aβ40 and Aβ42 species in 5xFAD-Rag2KO, compared to 5xFAD-WT (Fig. 1-A). Soluble and insoluble Aβ40 and Aβ42 were undetectable in WT-WT and WT-Rag2ko mice. Sections of dentate gyrus (DG) and frontal cortex (FC) were also immunolabeled with 6E10 antibody to assess plaque load, using confocal microscopy (Fig. 1-B-C). As expected, 5xFAD-WT mice, at age 10-month, showed highly abundant plaques in the DG and FC. In comparison between 5xFAD-WT and 5xFAD-Rag2KO, while the number of plaques (Fig. 1-E&H) and their signal intensities (Fig. 1-F&I) were comparable, the absence of T, B and NK cells in 5xFAD-Rag2KO, further increased the percentage of area covered by Aβ in the DG (Fig. 1-D).

In the next step, CD4^{+}CD25^{high}Tregs were isolated from peripheral blood of a healthy human subject and expanded *ex vivo* for 24 days. Ex vivo expansion, substantially enhances immunoregulatory capacity of Tregs, as reported previously (22). Tregs vs. PBS were adoptively transferred by intravenous injection into the tail of 5xFAD-Rag2KO and WT-Rag2KO mice and the presence of Tregs in the murine brain was evaluated after 2 weeks with co-labeling against CD3 and Foxp3 as described previously (32). Human Tregs were detected in the DG and FC of 5xFAD-Rag2KO mice following peripheral administration, suggesting that these human cells survived in immunocompromised mice and distributed into the CNS (Fig. 1-J, supplementary Fig. 2). In quantifying number of Tregs in DG and FC (Fig. 1-K&L), there was a trend toward increased number of Tregs in the DG of Treg-treated 5xFAD-Rag2 ko compared to Treg-treated WT-Rag2 KO.

We next examined the effect of Tregs on AD pathology. Treg administration effectively reduced the levels of both soluble and insoluble Aβ40 and Aβ42 in 5xFAD-Rag2KO mice, compared to the untreated group (Fig. 1-A). Levels of soluble Aβ42 in Treg-treated 5xFAD-Rag2KO were even lower than in the immunocompetent 5xFAD-WT group. In immunohistochemical analysis, the total plaque area (Fig. 1D&G) and the number of plaques (Fig. 1-E&H) within the DG and FC of 5xFAD-Rag2KO mice were alleviated

following Treg administration. The signal intensity of plaques was also lowered in the Treg-treated AD group, suggesting reduced plaque compaction following Treg administration (Fig. 1-F&I).

Treg administration modifies glial cells in AD mice

Compared to WT, the 10-month-old 5xFAD-WT mice showed 2–3 folds increases in the number of $Iba1^+$ microglia in the DG and the FC. The total number of $Iba1^+$ microglia was comparable between 5xFAD-WT and 5xFAD-Rag2KO and remained unaltered after Treg administration (Fig. 2-A&B, supplementary Fig. 3-A&B). In evaluating number of microglia that were surrounding plaques (within 20-µm radius of the 6E10-positive plaques), there was a trend toward increased level of plaque associated $Iba1^+$ microglia in the DG of 5xFAD-Rag2KO mice, compared to 5xFAD-WT (Fig. 2-C). Treg administration significantly reduced plaque associated $Iba1^+$ microglia in both DG and FC (Figs. 2-C& supplementary Fig. 3-C). In the next step, the number of activated microglia was assayed in the DG and FC, using CD68 staining (Fig. 2-D& supplementary Fig. 3-D). The number of $CD68^+$ microglia within the DG was increased following elimination of T, B and NK cells in 5xFAD-Rag2KO mice, compared to 5xFAD-WT (Fig. 2-E). Treg treatment significantly reduced total and plaque associated $CD68^+$microglia in both DG (Fig. 2-E&F) and FC of 5xFAD-Rag2KO (Supplementary Fig. 3-E&F).

In the next step, reactive astrocytes were evaluated in the DG and FC, using GFAP staining. There were major differences in astrocyte state in AD relative to WT group, as number of $GFAP^+$ reactive astrocytes in 5xFAD mice were about 4 folds higher than WT mice in the DG and FC (Fig. 3A&F). While number of $GFAP^+$ reactive astrocytes were comparable between 5xFAD-WT and 5xFAD-RAG2 KO group, Treg treatment significantly alleviated number of $GFAP^+$ reactive astrocytes in both DG and FC of 5xFAD-Rag2 KO mice (Fig. 3-B&D). In evaluating plaque associated reactive astrocytes, there was a trend toward increased level of $GFAP^+$ reactive astrocytes that were located within 50 um of amyloid plaques in the DG and FC of 5xFAD-Rag2KO mice compared to 5xFAD-WT. Treg treatment suppressed plaque associated $GFAP^+$ reactive astrocytes in both DG and FC (Fig. 3-C&E).

Identification of differentially expressed inflammation genes following adaptive immune system modification

NanoString gene expression panel of 770 mouse immune factors was applied in the extracted RNA from the hippocampus of WT-WT, WT-Rag2KO, 5xFAD-WT, 5xFAD-Rag2KO and Treg-treated 5xFAD-Rag2KO. Comparing of 5xFAD-WT with WT-WT mice, 73 immune related genes were upregulated (Fold change (FC) > 1.5, $p < 0.05$) and only 4 genes were downregulated (FC < 0.66, $p < 0.05$) in AD mice (Fig. 4-A). Genes implicated in microglial/macrophage activation [*Clec7a*: FC = 14.7, *Ccl3*: FC = 11.7, *Cst7*: FC = 9.0, *Trem2*: FC = 5.4, *Tyrobp*: FC = 4.36, *CD68*: FC = 3.6] as well as complement activation (*Itgax*: FC = 5.5, *C4a*: FC = 4.2) were most highly upregulated in 10-month-old 5xFAD-WT mice, supporting the role of neuroinflammation in AD pathogenesis. Comparing 5xFAD-Rag2KO with WT-Rag2KO, 95 immune genes were upregulated and 7 genes were down-regulated in immunocompromised AD mice. Lack of T, B and NK cells in 5xFAD-Rag2KO further strengthened the pathological overexpression of

microglial/macrophage (*Clec7a*: FC = 19.0, *Cst7*: FC = 14.6, CCL3: FC = 11.3, *Trem2*: FC = 8.0, *Tyrobp*: FC = 7.0 and *CD68*: FC = 6.1) and complement activation (*Itgax*: FC = 8.1, *C4a*: FC = 6.2) markers (Fig. 4-B). Finally, we evaluated the impact of *ex vivo* expanded human Tregs on modulating neuroinflammation transcriptome. 91 out of 99 up or down-regulated genes in 5xFAD-Rag2KO, had opposite direction of fold changes following Treg treatment, which suggests Treg treatment is pulling the expression profile of these immune genes away from 5xFAD-Rag2KO and towards WT-Rag2KO (Fig. 4-C). Applying Ingenuity's pathway analysis, we interrogated these genes with respect to enriched network and subcellular compartments. The enriched network was centered in extracellular complements activation (*C1qa, C1qb, C1qc, C4a/b*) and pro-inflammatory cytokine networks (*IL1A&B, IL6, Tnfa, Ifnγ*) as well as membrane binding receptors of toll like receptors (*Tlr3, Tlr4* and *Tlr7*) and myeloid activation markers (*CD14, Tyrobp,Trem2, CD68*). In addition, nuclear localized binding motifs of the interferon-regulatory factors (*Irf3 and Irf7*) were enriched (Fig. 4-D). In order to verify the finding of pathway integrative analysis, 10 enriched genes including complement activation markers (C1qa, C1qb, C1qc), pro-inflammatory cytokines (IL1B, IL6, Tnfa), microglial activation markers (Tyrobp, Trem2) and transmembrane protein genes of Tlr and Itgax were selected for further confirmation using quantitative real-time PCR. 8 out of 10 selected genes were significantly upregulated in 5xFAD-RAG2 KO mice and down-regulated or had a trend toward reduced expressions following subsequent Treg administration (Fig. 4-E-O). Finally, anti-inflammatory cytokine expressions in the hippocampus were analyzed that expressed upregulation of IL-10 transcripts, following administration of Tregs into 5xFAD-RAG2 KO mice (Fig. 4-P-T).

Discussion:

Our study characterized the impact of *ex vivo* expanded human Tregs in a preclinical AD model. Following peripheral administration, human Tregs were detectable in the central nervous system of immunodeficient AD mice and reduced amyloid burden and reactive glial cells. Similar to our finding, systemic Treg expansion in AD transgenic mice models, including low dose IL-2 administration, modified neuroinflammation and enhanced neuroprotection against AD pathology (33–35). However, these regulatory T cells might have dichotomous effects on the neurodegenerative process by obstructing a selective gateway for immune cell trafficking to the CNS, reducing the recruitment of immunoregulatory cells from the periphery to the CNS particularly in juvenile mice (36). However, we believe that in older AD mice in the presence of AD pathology or in the clinical setting of Alzheimer's disease, the structural integrity of the blood-brain barrier has already broken down and peripheral immune cells would migrate through the activated endothelium by various mechanisms.

We initially generated immunocompromised AD mice model with lack of adaptive immune system. Genetic ablation of T cells, B cells and NK cells in AD mice, further amplified the expression of pathologic inflammatory genes involved in complement cascade and microglial activation. The activation of complement cascade and pro-inflammatory microglia can lead to synaptic dysfunction, neuronal death and inhibition of neurogenesis (37–39). The upregulation of these neuroinflammatory networks and increased number of activated glial cells in this study were associated with accelerated amyloid plaque deposition, as reported previously (40). In contrast to Our finding and Marsh et al. study that applied Rag2

Il2rγ$^{-/-}$ double knock out in 5xFAD mice (Lack of B, T and NKC), Späni et al. used single knock out Rag2 PSAPP transgenic mice (NKC sufficient) with contradicting reduction in CNS amyloid burden (41). Together, these results indicate that NK cells might play a considerable role in microglial activation and amyloid pathology.

Accumulating preclinical and clinical evidences suggest that adaptive transfer of ex vivo expanded Tregs is a novel therapeutic strategy to modulate chronic inflammation in neurodegenerative processes (23). Following ex vivo expansion, the immunophenotype and suppressive function of ex vivo expanded Tregs would be substantially restored and amplified. While “baseline” Tregs are extremely heterogeneous, ex vivo expanded Tregs from healthy controls as well as AD individuals have comparable proteomic profiles, FoxP3 expression, and functional suppression of pro-inflammatory myeloid cells and T responder proliferation (22). In the current study, we investigated the modulatory effect of ex vivo expanded human Treg with amplified immunosuppressive function on AD pathology in a preclinical AD mice model. The 5xFAD-Rag2KO mice lack T cells, B cells and natural killer cells, key immune components involved in xenogeneic cell rejection and are suitable for engraftment of human cells without preconditioning (26–31, 42–44). Following peripheral administration, Tregs were detectable in the hippocampus and frontal cortex of mice. This finding is consistent with previous study that has shown survival of human Treg in immunocompromised mice for at least 40 days after administration (45) and also supported transmigration of peripheral Tregs into the CNS (35, 46, 47). However, further studies are still required to assess the detailed distribution and immunophenotypic persistence of adoptively transferred Treg following peripheral administration. In addition, an important limitation in interpretation of our finding is the unknown extend of cross-reactivity between ex vivo expanded human Tregs immunomodulatory markers and mice immune system which might affect the biologic function of human Treg in immunocompromised 5xFAD-Rag2KO mice. Absence of the IL-2Rγ-chain in 5xFAD-Rag2KO mice also results in a lack of cytokines functions and might further limit the immunomodulatory function of human Tregs in these immunocompromised mice.

Microglia are one of the initial responders to amyloid-β plaque deposits (4–6). While, low concentrations of Aβ can be taken up by microglia and concentrated into acidic vesicles. Excessive accumulation of Aβ within microglial lysosomes might induce cellular death, potentially contributing to plaque expansion through the release of Aβ aggregates at the site of microglial death (48). In this context, other studies identified roles of activated inflammatory microglia in initiating and expanding plaque pathogenesis rather than phagocytosis and removal (48–51). In our study, Treg administration to 5xFAD-Rag2KO mice, did not alter overall microgliosis but did reduce the number of reactivate microglia surrounding the plaques.

Astroglia are thought to be the most prevalent cell type in the brain (52, 53). Aβ oligomers and inflammatory mediators transform resting astrocytes to hyperplastic and hypertrophic GFAP-high disease associated astrocytes which secrete further pro-inflammatory cytokines and upregulate APP expression (54–56). In a recent study, adaptive transfer of Tregs into Rag2 KO mice suppressed neurotoxic astrogliosis in the chronic phase of stroke (32). Our data expands this finding to AD pathology as Treg

therapy effectively alleviated total and plaque associated $GFAP^+$ reactive astrocytes in both dentate gyrus and frontal cortex.

Finally, the pathologic upregulation of inflammation genes in 5xFAD-Rag2KO was modified following Treg administration. Using Ingenuity Pathway Analysis, we noted that the enriched pathways were mainly associated with down-regulation of pro-inflammatory cytokines (*IL1A&B, IL6*), complement cascade (*C1qa, C1qb, C4a/b*), toll like receptors (*Tlr3, Tlr4* and *Tlr7*) and microglial activations markers (*CD14, Tyrobp,Trem2*). These canonical signaling pathways are mainly reported as part of "microglial pro-inflammatory responses" to toxic Aβ (57). We propose that reduced number of plaque-associated glial cells and suppression of pro-inflammatory signaling pathways within these cells following Treg therapy have attenuated the contribution of these toxic glial cells in AD pathology and mitigated amyloid burden.

Conclusion:

In this study ex vivo expanded human Tregs were adaptively transferred to immunodeficient 5xFAD-Rag2KO mice. Following peripheral administration, Tregs were detectable in the central nervous system, suppressed neuroinflammation and substantially alleviated amyloid pathogenesis. These promising preclinical findings provide a rationale for enhancing Treg immunomodulatory function with infusions of ex vivo expanded Tregs or in vivo expansion of endogenous Tregs in patients with Alzheimer's disease.

Abbreviations:

AD: Alzheimer's Disease; ALS: Amyotrophic Lateral Sclerosis; CNS: Central Nervous System; FA: Formic Acid; FC: Fold Change; IPA: Ingenuity Pathway Analysis; iPCS: induced Pluripotent Stem Cells; MFI: Mean Fluorescence Intensities NK: Natural Killer; Treg: Regulatory T cells; Tresp: T responders; TLR: toll-like receptors; WT: Wild Type;

Declarations:

Ethics approval and consent to participate:

Approvals were from the Methodist Research Institute's Institutional Animal Care and Use Committee.

Consent for publication:

This manuscript has been read and approved by all authors, it has not been previously published, and is not under simultaneous consideration by another journal. Authors give consent for publication in Molecular Neurodegeneration.

Availability of supporting data:

The datasets supporting the conclusions of this article are included within the article and its additional supplementary file. The other raw and analysed datasets generated during the study are available for

research purposes from the corresponding author on reasonable request.

Competing interests:

The authors of this manuscript declare that they have no competing interests.

Funding:

This research was supported by a BrightFocus foundation fellowship award and an award from the Houston Methodist Clinician Scientist Recruitment and Retention Program.

Author's contributions:

AF, JCM and SHA conceived and designed research; AF, ADT, HX, JHW, XL, SW, JRT, WZ, DRB performed 5xFAD-RAG2 studies; AF, MV and HZ performed confocal microscopy analysis, Computational analysis of the RNA-seq data was performed at gene expression level by AF, ZY and STW. AF wrote manuscript with input from all authors. All authors read and approved the final version of the manuscript.

Acknowledgements:

Acknowledgement is made to the donors of Alzheimer's Disease Research, a program of the BrightFocus Foundation. We are grateful to the Nantz National Alzheimer Center donors for making this research possible. We want to thank Houston Methodist Research Institute's Advanced Cellular and Tissue Microscopy Core Facility for the support.

References:

1. Schwartzentruber J, Cooper S, Liu JZ, Barrio-Hernandez I, Bello E, Kumasaka N, et al. Genome-wide meta-analysis, fine-mapping and integrative prioritization implicate new Alzheimer's disease risk genes. Nat Genet. 2021;53(3):392–402.
2. Jansen IE, Savage JE, Watanabe K, Bryois J, Williams DM, Steinberg S, et al. Genome-wide meta-analysis identifies new loci and functional pathways influencing Alzheimer's disease risk. Nat Genet. 2019;51(3):404–13.
3. McQuade A, Blurton-Jones M. Microglia in Alzheimer's Disease: Exploring How Genetics and Phenotype Influence Risk. J Mol Biol. 2019;431(9):1805–17.
4. Welikovitch LA, Do Carmo S, Magloczky Z, Malcolm JC, Loke J, Klein WL, et al. Early intraneuronal amyloid triggers neuron-derived inflammatory signaling in APP transgenic rats and human brain. Proc Natl Acad Sci U S A. 2020;117(12):6844–54.
5. Masliah E, Sisk A, Mallory M, Mucke L, Schenk D, Games D. Comparison of neurodegenerative pathology in transgenic mice overexpressing V717F beta-amyloid precursor protein and Alzheimer's disease. J Neurosci. 1996;16(18):5795–811.

6. Jung CK, Keppler K, Steinbach S, Blazquez-Llorca L, Herms J. Fibrillar amyloid plaque formation precedes microglial activation. PLoS ONE. 2015;10(3):e0119768.
7. Venegas C, Kumar S, Franklin BS, Dierkes T, Brinkschulte R, Tejera D, et al. Microglia-derived ASC specks cross-seed amyloid-beta in Alzheimer's disease. Nature. 2017;552(7685):355–61.
8. Liu Y, Dai Y, Li Q, Chen C, Chen H, Song Y, et al. Beta-amyloid activates NLRP3 inflammasome via TLR4 in mouse microglia. Neurosci Lett. 2020;736:135279.
9. Nakanishi A, Kaneko N, Takeda H, Sawasaki T, Morikawa S, Zhou W, et al. Amyloid beta directly interacts with NLRP3 to initiate inflammasome activation: identification of an intrinsic NLRP3 ligand in a cell-free system. Inflamm Regen. 2018;38:27.
10. Lonnemann N, Hosseini S, Marchetti C, Skouras DB, Stefanoni D, D'Alessandro A, et al. The NLRP3 inflammasome inhibitor OLT1177 rescues cognitive impairment in a mouse model of Alzheimer's disease. Proc Natl Acad Sci U S A. 2020;117(50):32145–54.
11. Ising C, Venegas C, Zhang S, Scheiblich H, Schmidt SV, Vieira-Saecker A, et al. NLRP3 inflammasome activation drives tau pathology. Nature. 2019;575(7784):669–73.
12. Nilson AN, English KC, Gerson JE, Barton Whittle T, Nicolas Crain C, Xue J, et al. Tau Oligomers Associate with Inflammation in the Brain and Retina of Tauopathy Mice and in Neurodegenerative Diseases. J Alzheimers Dis. 2017;55(3):1083–99.
13. van Olst L, Verhaege D, Franssen M, Kamermans A, Roucourt B, Carmans S, et al. Microglial activation arises after aggregation of phosphorylated-tau in a neuron-specific P301S tauopathy mouse model. Neurobiol Aging. 2020;89:89–98.
14. Di J, Cohen LS, Corbo CP, Phillips GR, El Idrissi A, Alonso AD. Abnormal tau induces cognitive impairment through two different mechanisms: synaptic dysfunction and neuronal loss. Sci Rep. 2016;6:20833.
15. Montagne A, Zhao Z, Zlokovic BV. Alzheimer's disease: A matter of blood-brain barrier dysfunction? J Exp Med. 2017;214(11):3151–69.
16. Montagne A, Nation DA, Sagare AP, Barisano G, Sweeney MD, Chakhoyan A, et al. APOE4 leads to blood-brain barrier dysfunction predicting cognitive decline. Nature. 2020;581(7806):71–6.
17. van de Haar HJ, Burgmans S, Jansen JF, van Osch MJ, van Buchem MA, Muller M, et al. Blood-Brain Barrier Leakage in Patients with Early Alzheimer Disease. Radiology. 2017;282(2):615.
18. Gate D, Saligrama N, Leventhal O, Yang AC, Unger MS, Middeldorp J, et al. Clonally expanded CD8 T cells patrol the cerebrospinal fluid in Alzheimer's disease. Nature. 2020;577(7790):399–404.
19. Xie L, Choudhury GR, Winters A, Yang SH, Jin K. Cerebral regulatory T cells restrain microglia/macrophage-mediated inflammatory responses via IL-10. Eur J Immunol. 2015;45(1):180–91.
20. Rosenzweig N, Dvir-Szternfeld R, Tsitsou-Kampeli A, Keren-Shaul H, Ben-Yehuda H, Weill-Raynal P, et al. PD-1/PD-L1 checkpoint blockade harnesses monocyte-derived macrophages to combat cognitive impairment in a tauopathy mouse model. Nat Commun. 2019;10(1):465.

21. Kramer TJ, Hack N, Bruhl TJ, Menzel L, Hummel R, Griemert EV, et al. Depletion of regulatory T cells increases T cell brain infiltration, reactive astrogliosis, and interferon-gamma gene expression in acute experimental traumatic brain injury. J Neuroinflammation. 2019;16(1):163.
22. Faridar A, Thome AD, Zhao W, Thonhoff JR, Beers DR, Pascual B, et al. Restoring regulatory T-cell dysfunction in Alzheimer's disease through ex vivo expansion. Brain Commun. 2020;2(2):fcaa112.
23. Thonhoff JR, Beers DR, Zhao W, Pleitez M, Simpson EP, Berry JD, et al. Expanded autologous regulatory T-lymphocyte infusions in ALS: A phase I, first-in-human study. Neurol Neuroimmunol Neuroinflamm. 2018;5(4):e465.
24. Landel V, Baranger K, Virard I, Loriod B, Khrestchatisky M, Rivera S, et al. Temporal gene profiling of the 5XFAD transgenic mouse model highlights the importance of microglial activation in Alzheimer's disease. Mol Neurodegener. 2014;9:33.
25. Oblak AL, Lin PB, Kotredes KP, Pandey RS, Garceau D, Williams HM, et al. Comprehensive Evaluation of the 5XFAD Mouse Model for Preclinical Testing Applications: A MODEL-AD Study. Front Aging Neurosci. 2021;13:713726.
26. Wu DC, Hester J, Nadig SN, Zhang W, Trzonkowski P, Gray D, et al. Ex vivo expanded human regulatory T cells can prolong survival of a human islet allograft in a humanized mouse model. Transplantation. 2013;96(8):707–16.
27. Allen TM, Brehm MA, Bridges S, Ferguson S, Kumar P, Mirochnitchenko O, et al. Humanized immune system mouse models: progress, challenges and opportunities. Nat Immunol. 2019;20(7):770–4.
28. Bertilaccio MT, Scielzo C, Simonetti G, Ponzoni M, Apollonio B, Fazi C, et al. A novel Rag2-/-gammac-/–xenograft model of human CLL. Blood. 2010;115(8):1605–9.
29. Lee K, Kwon DN, Ezashi T, Choi YJ, Park C, Ericsson AC, et al. Engraftment of human iPS cells and allogeneic porcine cells into pigs with inactivated RAG2 and accompanying severe combined immunodeficiency. Proc Natl Acad Sci U S A. 2014;111(20):7260–5.
30. Mutis T, van Rijn RS, Simonetti ER, Aarts-Riemens T, Emmelot ME, van Bloois L, et al. Human regulatory T cells control xenogeneic graft-versus-host disease induced by autologous T cells in RAG2-/-gammac-/- immunodeficient mice. Clin Cancer Res. 2006;12(18):5520–5.
31. Vahedi F, Nham T, Poznanski SM, Chew MV, Shenouda MM, Lee D, et al. Ex Vivo Expanded Human NK Cells Survive and Proliferate in Humanized Mice with Autologous Human Immune Cells. Sci Rep. 2017;7(1):12083.
32. Ito M, Komai K, Mise-Omata S, Iizuka-Koga M, Noguchi Y, Kondo T, et al. Brain regulatory T cells suppress astrogliosis and potentiate neurological recovery. Nature. 2019;565(7738):246–50.
33. Dansokho C, Ait Ahmed D, Aid S, Toly-Ndour C, Chaigneau T, Calle V, et al. Regulatory T cells delay disease progression in Alzheimer-like pathology. Brain. 2016;139(Pt 4):1237–51.
34. Baek H, Ye M, Kang GH, Lee C, Lee G, Choi DB, et al. Neuroprotective effects of CD4 + CD25 + Foxp3 + regulatory T cells in a 3xTg-AD Alzheimer's disease model. Oncotarget. 2016;7(43):69347–57.
35. Alves S, Churlaud G, Audrain M, Michaelsen-Preusse K, Fol R, Souchet B, et al. Interleukin-2 improves amyloid pathology, synaptic failure and memory in Alzheimer's disease mice. Brain.

2017;140(3):826–42.

36. Baruch K, Rosenzweig N, Kertser A, Deczkowska A, Sharif AM, Spinrad A, et al. Breaking immune tolerance by targeting Foxp3(+) regulatory T cells mitigates Alzheimer's disease pathology. Nat Commun. 2015;6:7967.
37. Mishra A, Kim HJ, Shin AH, Thayer SA. Synapse loss induced by interleukin-1beta requires pre- and post-synaptic mechanisms. J Neuroimmune Pharmacol. 2012;7(3):571–8.
38. Hong S, Beja-Glasser VF, Nfonoyim BM, Frouin A, Li S, Ramakrishnan S, et al. Complement and microglia mediate early synapse loss in Alzheimer mouse models. Science. 2016;352(6286):712–6.
39. Leng F, Edison P. Neuroinflammation and microglial activation in Alzheimer disease: where do we go from here? Nat Rev Neurol. 2021;17(3):157–72.
40. Marsh SE, Abud EM, Lakatos A, Karimzadeh A, Yeung ST, Davtyan H, et al. The adaptive immune system restrains Alzheimer's disease pathogenesis by modulating microglial function. Proc Natl Acad Sci U S A. 2016;113(9):E1316-25.
41. Spani C, Suter T, Derungs R, Ferretti MT, Welt T, Wirth F, et al. Reduced beta-amyloid pathology in an APP transgenic mouse model of Alzheimer's disease lacking functional B and T cells. Acta Neuropathol Commun. 2015;3:71.
42. McQuade A, Kang YJ, Hasselmann J, Jairaman A, Sotelo A, Coburn M, et al. Gene expression and functional deficits underlie TREM2-knockout microglia responses in human models of Alzheimer's disease. Nat Commun. 2020;11(1):5370.
43. Claes C, Danhash EP, Hasselmann J, Chadarevian JP, Shabestari SK, England WE, et al. Plaque-associated human microglia accumulate lipid droplets in a chimeric model of Alzheimer's disease. Mol Neurodegener. 2021;16(1):50.
44. Espuny-Camacho I, Arranz AM, Fiers M, Snellinx A, Ando K, Munck S, et al. Hallmarks of Alzheimer's Disease in Stem-Cell-Derived Human Neurons Transplanted into Mouse Brain. Neuron. 2017;93(5):1066-81 e8.
45. Jacob J, Nadkarni S, Volpe A, Peng Q, Tung SL, Hannen RF, et al. Spatiotemporal in vivo tracking of polyclonal human regulatory T cells (Tregs) reveals a role for innate immune cells in Treg transplant recruitment. Mol Ther Methods Clin Dev. 2021;20:324–36.
46. Zhang H, Xia Y, Ye Q, Yu F, Zhu W, Li P, et al. In Vivo Expansion of Regulatory T Cells with IL-2/IL-2 Antibody Complex Protects against Transient Ischemic Stroke. J Neurosci. 2018;38(47):10168–79.
47. Shi L, Sun Z, Su W, Xu F, Xie D, Zhang Q, et al. Treg cell-derived osteopontin promotes microglia-mediated white matter repair after ischemic stroke. Immunity. 2021;54(7):1527-42 e8.
48. Spangenberg E, Severson PL, Hohsfield LA, Crapser J, Zhang J, Burton EA, et al. Sustained microglial depletion with CSF1R inhibitor impairs parenchymal plaque development in an Alzheimer's disease model. Nat Commun. 2019;10(1):3758.
49. Baik SH, Kang S, Son SM, Mook-Jung I. Microglia contributes to plaque growth by cell death due to uptake of amyloid beta in the brain of Alzheimer's disease mouse model. Glia. 2016;64(12):2274–90.

50. Leyns CEG, Ulrich JD, Finn MB, Stewart FR, Koscal LJ, Remolina Serrano J, et al. TREM2 deficiency attenuates neuroinflammation and protects against neurodegeneration in a mouse model of tauopathy. Proc Natl Acad Sci U S A. 2017;114(43):11524–9.
51. Dani M, Wood M, Mizoguchi R, Fan Z, Walker Z, Morgan R, et al. Microglial activation correlates in vivo with both tau and amyloid in Alzheimer's disease. Brain. 2018;141(9):2740–54.
52. Sofroniew MV, Vinters HV. Astrocytes: biology and pathology. Acta Neuropathol. 2010;119(1):7–35.
53. Frost GR, Li YM. The role of astrocytes in amyloid production and Alzheimer's disease. Open Biol. 2017;7(12).
54. Habib N, McCabe C, Medina S, Varshavsky M, Kitsberg D, Dvir-Szternfeld R, et al. Disease-associated astrocytes in Alzheimer's disease and aging. Nat Neurosci. 2020;23(6):701–6.
55. Blasko I, Veerhuis R, Stampfer-Kountchev M, Saurwein-Teissl M, Eikelenboom P, Grubeck-Loebenstein B. Costimulatory effects of interferon-gamma and interleukin-1beta or tumor necrosis factor alpha on the synthesis of Abeta1-40 and Abeta1-42 by human astrocytes. Neurobiol Dis. 2000;7(6 Pt B):682–9.
56. Hou L, Liu Y, Wang X, Ma H, He J, Zhang Y, et al. The effects of amyloid-beta42 oligomer on the proliferation and activation of astrocytes in vitro. In Vitro Cell Dev Biol Anim. 2011;47(8):573–80.
57. Rodriguez-Gomez JA, Kavanagh E, Engskog-Vlachos P, Engskog MKR, Herrera AJ, Espinosa-Oliva AM, et al. Microglia: Agents of the CNS Pro-Inflammatory Response. Cells. 2020;9(7).

Figures

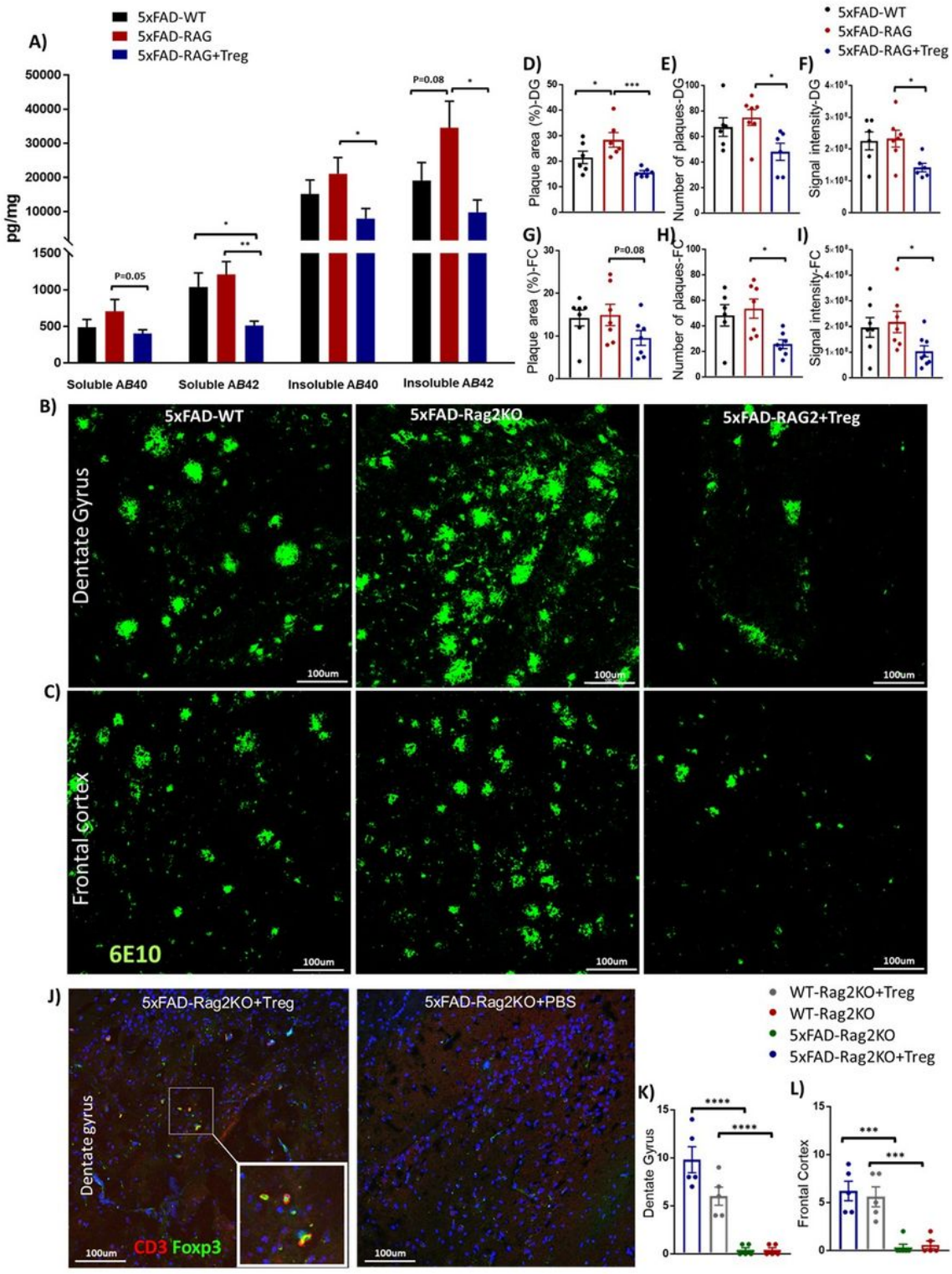

Figure 1

Treg treatment suppress Amyloid pathology. (A) ELISA quantification of mice brain homogenates shows a trend toward an increased levels of SDS-soluble and formic acid treated insoluble Aβ40 and Aβ42 in 5xFAD-Rag2KO, compared to 5xFAD-WT. Human *ex vivo* expanded Treg administration decreased both soluble and insoluble Aβ40 and Aβ42 burden in 5xFAD-Rag2KO (10-month-old mice, 10 per group; sex-balanced). **(B-C)** Representative images of Aβ immunostaining (6E10) of the dentate gyrus (DG) and

frontal cortex (FC) in 5xFAD-WT, 5xFAD-Rag2KO and Treg-treated 5xFAD-Rag2KO. **(D-I)** Quantification of the 6E10-positive amyloid aggregates in the DG and FC. The percentage of area covered by Aβ in the DG were increased in 5xFAD-Rag2KO compared to 5xFAD-WT. Number of plaques and their signal intensity were comparable between 5xFAD-Rag2KO and 5xFAD-WT in both DG and FC. Human ex vivo expanded Treg administration reduced area covered by plaque, number of plaques and their signal intensity in both DG and FC of 5xFAD-Rag2ko mice (n=6 per group, sex balanced). **(J)** Immunostaining of Tregs (CD3 in red, Foxp3 in green) and cell nuclei (DAPI in blue) in the DG of 10-month-old 5xFAD-Rag2KO mice treated with human Tregs or Phosphate-buffered saline (PBS). **(K-L)** Quantification of number of $CD3^{+}Foxp3^{+}$ Tregs in the DG and FC of 4 groups of mice including Treg treated 5xFAD-Rag2KO, Treg treated WT-Rag2KO, PBS treated 5xFAD-Rag2KO and also PBS treated WT-Rag2KO mice. Numbers shown as averages ± SEM with one-way ANOVA. P-values are *p < 0.05, **p< 0.01, ***p< 0.001, ****p< 0.0001. Scale bar, 100 μm.

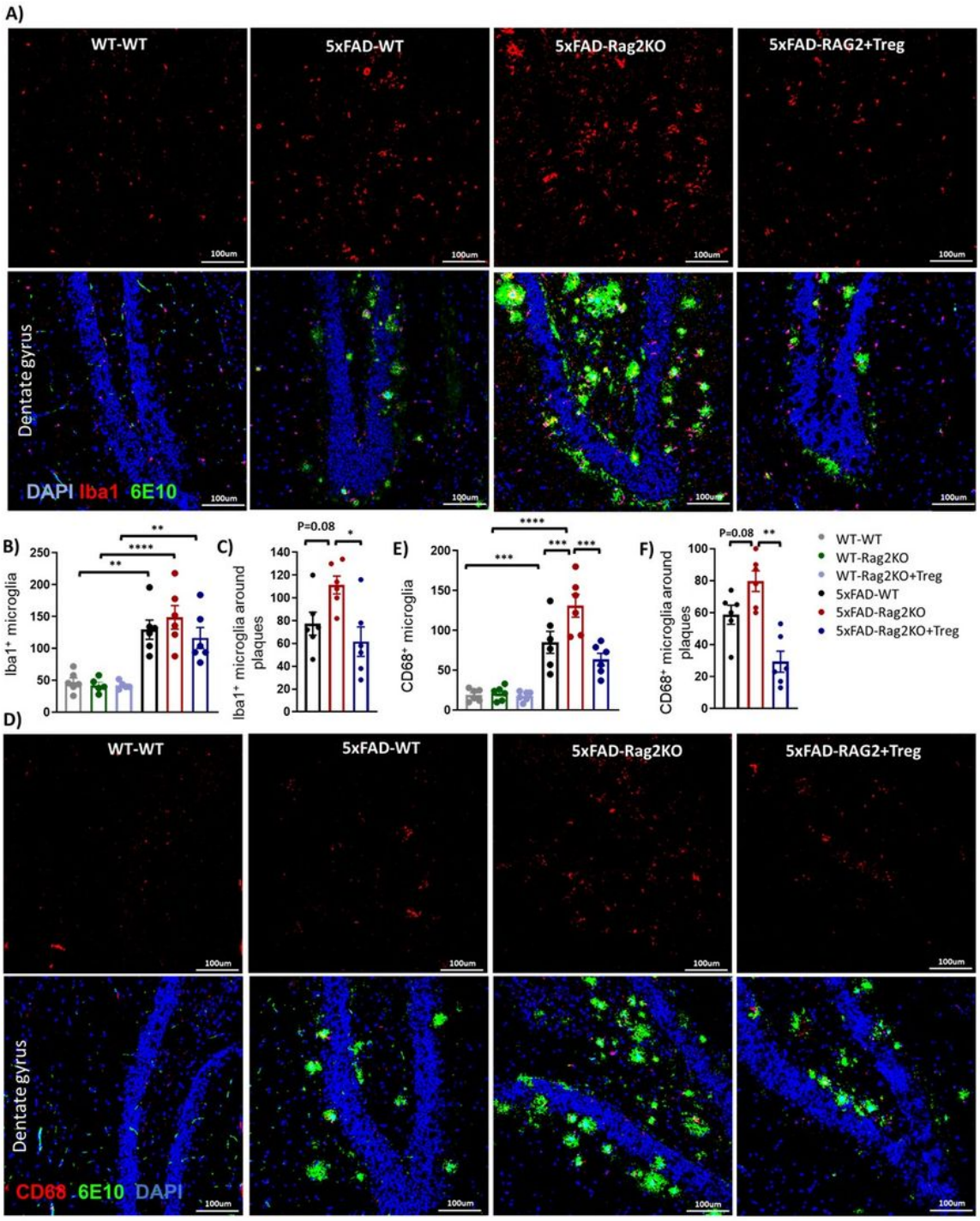

Figure 2

Treg administration reduces number of activated microglia in the dentate gyrus. (A) Representative images of Iba1 positive-microglia (red) and 6E10-positive Aβ plaques (green) in the dentate gyrus (DG) of WT-WT, 5xFAD-WT, 5xFAD-Rag2KO and Treg-treated 5xFAD-Rag2KO (n = 6 per group, sex balanced). **(B)** Quantification of the number of Iba^{+} microglia in the DG; while number of Iba1^{+}microglia was increased in 5xFAD-WT mice, compared to WT-WT, lack of adaptive immune system in 5xFAD-Rag2KO and

subsequent Treg administration had no effect on the number of Iba1^{+} microglia. **(C)** Quantification of the number of Iba1^{+} microglia within 20 um of the plaque surface; Treg administration reduced number of plaque-associated Iba1^{+} microglia. **(D)** Representative images of CD68-positive activated microglia (red) and 6E10-positive Aβ plaques (green) in the dentate gyrus. Quantification of CD68-positive activated microglia **(E)** in the DG and CD68-positive microglia within 20 um of the plaque surface **(F)**, revealed decreased number of total and plaque-associated CD68^{+} microglia in 5xFAD-Rag2KO following Treg administration. Numbers shown as averages ± SEM with one-way ANOVA. *P < 0.05, **P < 0.01, ***P < 0.001 and ****p< 0.0001. Scale bar, 100 μm.

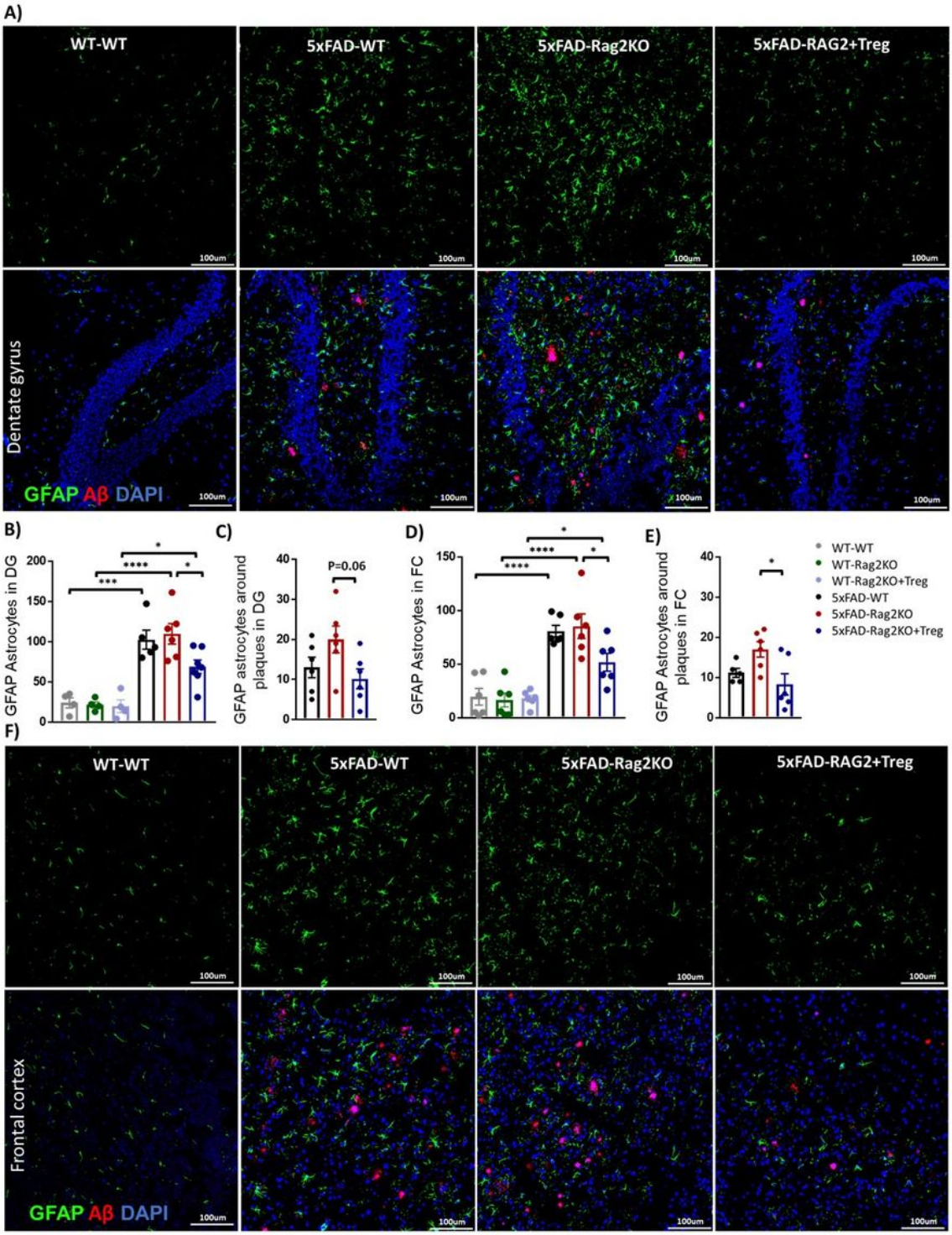

Figure 3

Treg administration reduces number of reactive astrocytes. Representative images of GFAP positive-reactive astrocytes (green) and Aβ 1-42 positive plaques (red) in the dentate gyrus (DG) **(A)** and frontal cortex (FC) **(F)** of WT-WT, 5xFAD-WT, 5xFAD-Rag2KO and Treg-treated 5xFAD-Rag2KO (n = 6 per group, sex balanced). **(B-E)** Quantification of the number of $GFAP^+$ reactive astrocytes in the DG and FC; number of $GFAP^+$ reactive astrocytes was increased in 5xFAD-WT mice, compared to WT-WT. Lack of adaptive

immune system in 5xFAD-Rag2KO had no effect on the number of GFAP^{+} reactive astrocytes, compared to 5xFAD-WT. Decreased number of total and plaque-associated GFAP^{+} reactive astrocytes in 5xFAD-Rag2KO were noted following Treg administration. Numbers shown as averages ± SEM with one-way ANOVA. *P < 0.05, **P < 0.01, ***P < 0.001 and ****p< 0.0001. Scale bar, 100 µm.

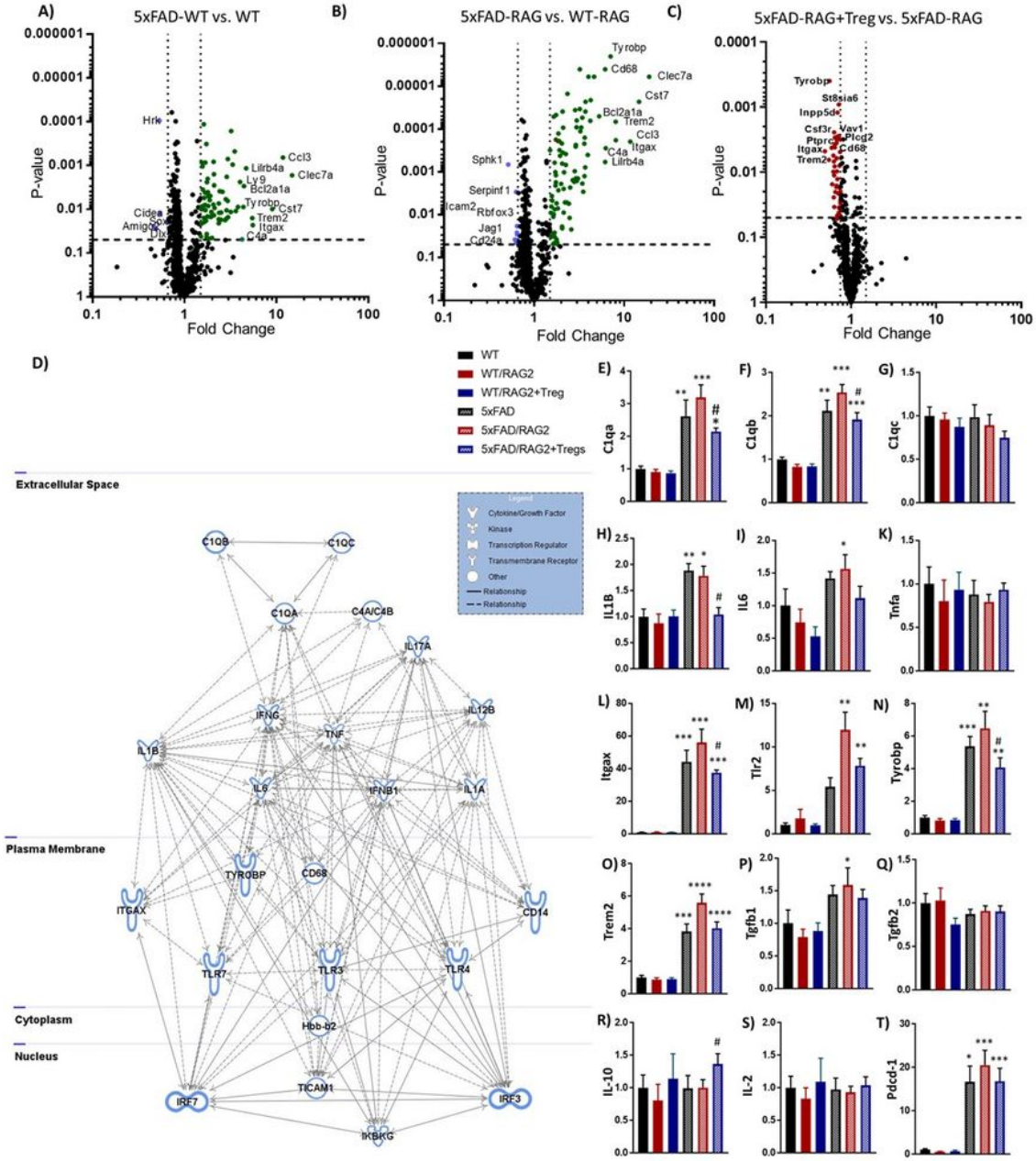

Figure 4

Modification of inflammation network following Treg administration. Volcano Plots showing fold changes vs. p-values of nCounter Mouse Neuroinflammation panel in **(A)** 5xFAD-WT vs. WT-WT**;** 73 immune related genes were upregulated (green dots) and 4 genes were down regulated (blue dots) in 5xFAD-WT (n=4 in each groups). **(B)** Compared with WT-Rag2KO, 95 genes were upregulated (green dots) and 7 genes were down-regulated (blue dots) in 5xFAD-Rag2KO. The 10 most upregulated genes and all down-regulated genes are labeled in the figures. **(C)** Treg-treated 5xFAD-Rag2KO vs. 5xFAD-Rag2KO; the pathologic upregulation of inflammation related genes in 5xFAD-Rag2KO were modified following Treg administration . **(D)** The network representation and subcellular assignment of the enriched pathway in Treg-treated 5xFAD-Rag2KO vs. untreated 5xFAD-Rag2KO. The enriched network were centered in down-regulation of pro-inflammatory cytokines (*IL1A&B, IL6, Tnfa, IFNγ*), complement activation (*C1qa, C1qb, C1qc, C4a/b*), toll like receptors (*Tlr3, Tlr4* and *Tlr7*), myeloid activation markers (*CD14, Tyrobp,Trem2*) and intra-nuclear binding motifs of interferon-regulatory factors (*IRF3* and *IRF7*). **(E-T)** Real time-PCR analysis of complement activation (C1qa, C1qb, C1qc), pro-inflammatory cytokines (IL1B, IL6, TNFa), microglial activation markers (Tyrobp, Trem2), transmembrane protein genes (TLR2 and Itgax) and anti-inflammatory cytokines (Tgfb1, Tgfb2, IL-10, IL-2, Pdcd1) transcripts. Numbers shown as averages ± SEM with one-way ANOVA. *comparison between each AD groups versus corresponding WT ones: *P < 0.05, **P < 0.01, ***P < 0.001 and ****p< 0.0001. **#** p<0.05 comparison between Treg treated-5xFAD-Rag2KO versus 5xFAD-Rag2KO groups.

Supplementary Files

This is a list of supplementary files associated with this preprint. Click to download.

- SupplementaryMaterial.docx